# Detailed analyses of stall force generation in *Mycoplasma mobile* gliding

**Masaki Mizutani[a], Isil Tulum[a,b], Yoshiaki Kinosita[c], Takayuki Nishizaka[c] and Makoto Miyata[a,b]**

[a] Graduate School of Science, Osaka City University, 3-3-138 Sugimoto, Sumiyoshi-ku, Osaka 558-8585, Japan

[b] The OCU Advanced Research Institute for Natural Science and Technology (OCARINA), Osaka City University, 3-3-138 Sugimoto, Sumiyoshi-ku, Osaka 558-8585, Japan

[c] Department of Physics, Faculty of Science, Gakushuin University, 1-5-1 Mejiro, Toshima-ku, Tokyo 171-8588, Japan

Corresponding author: (Makoto Miyata, Graduate School of Science, Osaka City University, 3-3-138 Sugimoto, Sumiyoshi-ku, Osaka 558-8585, Japan, +81-6-6605-3157, miyata@sci.osaka-cu.ac.jp)

Key words: gliding motility, optical tweezers, force measurement, gear ratio, energy conversion

## Abstract

*Mycoplasma mobile* glides on solid surfaces at a velocity of up to 4.5 μm/s with a unique mechanism. The gliding machinery composed of hundreds of units generates the force for gliding based on the energy of ATP, and catches and pulls the sialylated oligosaccharides fixed on solid surfaces. In the present study, we measured the stall force of a wild type and mutant strains of *M. mobile* carrying a bead manipulated by using optical tweezers. The strains enhanced for binding showed weaker stall force than the wild-type strain, indicating that the stall force is related to the step of force generation rather than binding. The stall force of the wild-type strain decreased linearly from 113 to 19 pN by the addition of free sialyllactose, a sialylated oligosaccharide from 0 to 0.5 mM with decreasing the number of working units. In the 0.5 mM sialyllactose conditions, the cells carrying a bead loaded by the optical tweezers showed stepwise movements with force increments. The force increments distributed from 1 to 2 pN. Considering the 70-nm large step size, this small unit force may be explained by the large gear ratio involved in the gliding machinery of *M. mobile*.


## Significance

*Mycoplasma* is a group of bacteria parasitic for animals. Dozens of species glide on their host tissues for infection. The gliding machinery of *Mycoplasma mobile*, the fastest species includes intracellular motors and many legs on the cell surface. In the present study, we measured the force generation precisely by using strongly focused laser beam, called optical tweezers, in different conditions. The measurements suggested that the gliding machinery has a large gear ratio to achieve the fast gliding speed.

## Introduction

Class *Mollicutes*, represented by *Mycoplasma* is parasitic and occasionally commensal bacteria that have small cell size, genomes, and no peptidoglycan layer (1, 2). Dozens of *Mycoplasma* species featured by protrusions, such as the fish pathogen *Mycoplasma mobile* (3-5) and the human pathogen *Mycoplasma pneumoniae* (6-8) exhibit gliding motility in the direction of the protrusion on solid surfaces, which is

involved in the parasitism of mycoplasmas. Interestingly, mycoplasma gliding has no relation with flagella, pili, other bacterial motility systems or conventional motor proteins that are common in eukaryotic motility.

*M. mobile*, isolated from the gills of a freshwater fish, is a fast-gliding mycoplasma (9-13). It glides smoothly and continuously on glass at an average speed of 2.0 to 4.5 μm/s, or three to seven times the length of the cell per second. The gliding mechanism of *M. mobile* has been studied and proposed a working model, called centipede or power-stroke model, by which the cells repeatedly catch, pull drag and release sialylated oligosaccharides (SOs) on solid surfaces (3-5, 14). The gliding machinery is composed of internal and surface structures (15-19). The internal structure includes the α- and β-subunit paralogs of F-type ATPase/synthase and generates the force for gliding, based on the energy of ATP (18-22). The force should be transmitted across the cell membrane to the surface structure, which is composed of at least three huge proteins, Gli123, Gli521 and Gli349 (15-17, 23). Gli521, the crank protein transmits the force from the cell inside to Gli349 with actual structural changes (17, 24). Gli349, the leg protein extends after thermal fluctuation and catches SOs which is the major structures on animal cell surfaces (Fig 1*A*) (9, 25-27). The cells always glide in the direction of the machinery, which may be caused by the directed binding of cells on solid surfaces (3, 28). Hundreds of gliding units existing on the cell should function cooperatively to achieve smooth gliding (Fig. 1*B*) (15, 27, 29). To examine this working model in detail, the behaviors of individual units should be clarified.

Recently, the discrete movements of gliding motility, possibly single leg movement was observed by controlling the working leg number through addition of free SOs (22, 27). Now, we focus on the pulling force exerted to the solid surface in the movements, because the force generation was not analyzed carefully for other than the final stall force of the wild-type strain (ref). In the present study, we quantitatively measured the force of whole cell of various strains under various conditions by using optical tweezers (11, 28, 30-32), and characterized the force generated by the gliding machinery.

## Results

**Stall force measurement.** To examine the force of *Mycoplasma mobile* gliding, we

84 measured a stall force by optical tweezers. Previously, the propelling force of *M.*
85 *mobile* cell was measured by using optical tweezers (11). The bead bound to the cell
86 was trapped by strongly focused laser beam and the force was calculated from the
87 distance between the centers of bead and trap because the force acting on the bead
88 increases linearly with the displacement from the trap center (11, 28, 32). In the
89 present study, *M. mobile* cells, biotinylated and suspended in phosphate-buffer saline
90 with glucose (PBS/G) were inserted into a tunnel chamber. Then, we added
91 1-μm-diameter polystyrene beads coated with avidin to the tunnel. A bead trapped by
92 optical tweezers was attached to the back end of the gliding cell through the
93 avidin-biotin interaction (28, 33, 34). The cell pulled the bead from the trap center
94 (Fig. 2*A* and Movie S1), and the pulling force increased from 0 s and reached the
95 plateau at around 40 s. The maximum values for average of 25 data points were used
96 as the stall force. The stall force of wild-type strain was 113 ± 32 pN ($n$ = 50).
97 To determine the proteins involved in force generation or force transmission, we
98 measured the stall force to compare with that of the wild-type strain, for six strains
99 which were previously isolated and featured for gliding speed and/or binding activity
100 (12, 21, 35). The *gli521* (P476R) mutant was reported to have a single amino acid
101 substitution from proline at 476th to arginine in Gli521 (21), and mutations in the other
102 strains have not been analyzed. The pulling forces of these mutants also increased
103 from 0 s and stalled at 20—50 s. The stall force of m14 strain, 110 ± 29 pN ($n$ = 29)
104 was not significantly different from that of the wild-type strain ($P$ = 0.1 > 0.05 by
105 Student's $t$-test). The stall forces of the *gli521* (P476R), m6, m27, m29 and m34
106 mutants were significantly reduced to 64%—81% of that of the wild-type strain ($P$ = 6
107 × $10^{-3}$, 4 × $10^{-4}$, 9 × $10^{-5}$, 8 × $10^{-9}$ and 4 × $10^{-4}$, respectively < 0.01 by Student's $t$-test)
108 (Fig. 2*B Inset*). The *gli521* (P476R) mutant featured by enhanced binding showed
109 smaller force than the wild-type strain, suggesting that the legs keep binding, not in
110 repetitive cycle of catch and release, in the stalled state.
111
112 **Genome sequencing of various strains.** To determine the proteins and mutations
113 associated with the decreases in the stall force, we sequenced the genomes of the strains
114 by using a next-generation sequencer, MiSeq. The genome of the *gli521* (P476R)

mutant was previously sequenced for a 30,469-bp DNA region encoding four open reading frames (ORFs), *gli123*, *gli349*, *gli521* and *gli42*, however, the other regions have not been sequenced (21). The genome sequencing result of the *gli521* (P476R) mutant was consistent with the previous report for the mutation in *gli521* (21) and also showed additional mutations in the new regions (Table 1). One of the additional mutations caused an amino acid substitution in MvspB, a surface protein (23, 36-39). However, the reduced stall force should be caused by the mutation in Gli521, because MvspB accounts for only 1.2% mass of all surface proteins and the antibody against a closely related abundant protein, MvspI did not influence the gliding motility (23, 39). The genomes of m6, m14, m27, m29 and m34 strains have not been sequenced yet, and we identified various mutations in the present study. The cause of the decreased stall force for m27 strain was suggested to be the mutation in *gli521* identified in the present study. All strains had the same single amino acid substitution from serine to isoleucine as 354th residue in MMOB1700, a homolog of ABC transporter permease based on BLAST search. This mutation may be derived from a substitution caused on the clone used for the reported genome sequencing, because the genome was sequenced for an isolate from the wild-type strain (ATCC 43663) being used in the present study (36). Interestingly, MMOB1700 showed other five different mutations in the 10 strains analyzed, suggesting a special mechanism causing high mutation rate in this gene. Next, we sequenced the genomes of nonbinding strains, m12, m13 and m23 which have been reported to have mutations in *gli123*, *gli349* and *gli349*, respectively (12, 15, 16, 35). The genome sequencing showed that the identified mutations were consistent with a previous report (35), although additional mutations were identified in other regions.

**Binding and gliding of various strains.** To clarify the relation between the features and mutation on the genome systematically, we examined the binding activities and the gliding speeds for the wild-type, *gli521* (P476R), m6, m14, m27, m29 and m34 mutants which can glide. The cell suspensions were adjusted to be the same optical density and inserted into a tunnel chamber. After 15 min, we video recorded the cells to count the numbers on a glass for bound-cell ratio and their gliding speed, as previously

reported (Fig. 3*A*) (29, 35, 40). The binding activities and the gliding speeds were averaged for 20 independent images and 100 cells, respectively. The binding activity and gliding speed of *gli521* (P476R) mutant were consistent with the previous study (35). Other strains have not been analyzed by the method used here. The characters of binding activities allowed classification of the strains into three types (Fig. 3*B* left). (i) m6 was 44% of that of the wild-type strain. (ii) m14, m27 and m29 were 80%, 92% and 73%, respectively. (iii) *gli521* (P476R) and m34 mutants were 159% and 145%, respectively. We compared these data to the binding activities which were previously estimated from hemadsorption, the adsorption of erythrocytes onto the surface of colonies (12). The hemadsorption of m6, m14, m27, m29 and m34 was 24%, 93%, 113%, 96% and 122%, respectively, consistent with the analyses in the present study, except m27. The gliding speed of the wild-type strain was 3.7 ± 0.2 μm/s and the mutants ranged from 80% to 103%, showing that the gliding speed differ less than the binding activities (Fig. 3*B* right). The strains enhanced for binding, the *gli521* (P476R) and m34 mutants had the reduced stall forces, suggesting that the stall force is not determined simply by binding activity.

Interestingly, we noticed that the proportions of nongliding bound cells are much higher in m6, m14, m27 and m29 strains than that of the wild-type strain. The proportions of gliding cells in the cells on glass were 94% for the wild-type strain as previously reported (40), but ranged 38%—84% in m6, m14, m27 and m29 strains (Fig. S1). This observation can be explained by assuming that the gliding can be achieved by harmonized actions of many molecules and interactions.

**Effect of SOs on stall force.** An *M. mobile* cell glides as a result of integrated movements for many legs. However, if the number of working legs is decreased, we may detect the pulling force of single unit. Previous studies showed that the number of working legs can be decreased by adding free SOs (9, 22, 25, 27, 40, 41). We therefore added various concentrations of free sialyllactose (SL), an SO, to gliding *M. mobile* cells and measured the stall force at 200 and 500 frames/s for the conditions of 0—0.25 and 0.33 and 0.5 mM free SL, respectively. The cells reached plateau by 30—40 s, and the time to reach the stall became longer with the concentration of free SL.

177 The stall force decreased from 113 to 19 pN with the addition up to 0.50 mM free SL
178 (Fig. 4*A* and *B*). These results suggest that the stall force is sum of the pulling force of
179 many units.
180
181 To detect the pulling force by smaller numbers of unit, we reduced the laser power of
182 optical tweezers to achieve higher resolution of the trace. In this experiment, we
183 applied 0.25 mM SL with the reduction of the trap stiffness of optical tweezers from 0.5
184 −0.7 to 0.1 pN/nm in which the trapped cells could escape from the trap center, and
185 measured the force under these conditions. The force increments with repeated small
186 peaks were detected, and the peaks were measured by a peak-finding algorithm and
187 summarized in Fig. 5*A*. The distribution of these increments was fitted by the sum of
188 four Gaussian curves whose peaks positioned at 1.1, 2.0, 3.2 and 4.4 pN (Fig. 5*B*).
189 The peaks positioned at twice, three and four times of the value of the first peak,
190 suggesting that these peaks may reflect single, double, triple and quadruple of the
191 minimum force increment (42). In the same way, the individual increments were
192 analyzed for the *gli521* (P476R) mutant and also fitted by the sum of four Gaussian
193 curves whose peaks positioned at 0.9, 1.8, 2.6 and 3.5 pN (Fig. 5*B*).
194
195 **Stepwise force increments.** **As** the force increments were detected under the
196 conditions of limited leg number, these force increments may be derived from the force
197 generation by a single leg or minimum force generation unit. Next, we added 0.50
198 mM SL to limit the number of working legs more with the reduction of the trap stiffness
199 to 0.06−0.07 pN/nm to detect the minimum force increments more precisely. As very
200 small ratio of cells remained on the glass surface under this condition, we attached a
201 bead to the cells by optical tweezers. Fifty one of 63 cells showed displacements.
202 Eight cells glided creeping displacements with occasional discontinuous increments,
203 which were mostly stepwise (Fig. 6*A*) and sometimes small peaks as shown in Fig 5.
204 Three cells showed continuous stepwise force increments (Fig. 6*B*). The average value
205 of force increments form 46 steps or peaks in 11 cell trajectories was 1.45 ± 0.44 pN
206 (Fig. 6*C*). These results suggest that the minimum force increment distributed from 1
207 to 2 pN, which should be the minimum unit force for gliding.

## Discussion

**Mutations influencing gliding.** In the present study, we sequenced the whole genomes of *M. mobile* mutants featured by binding ability, gliding motility and colony spreading. Based on these results, we propose the proteins responsible or related to these features. The m6 strain featured with reduced binding, slower gliding speed and weaker stall force has a mutation in FtsH, MvspI and SecY (37-39, 43, 44). The substituted amino acid in FtsH is not conserved in other mycoplasmas except *Mycoplasma pulmonis*, a closely related species. The MvspI is unlikely related to their gliding as described above (23). SecY is essential for protein secretion in bacteria, generally (44). The substitution in SecY probably should affect the secretion of gliding proteins, resulting in the reduction of binding activity of cells, because the substituted amino acid is conserved in many mycoplasmas, including *Mycoplasma hominis*, *Mycoplasma bovis*, and *M. pulmonis*. The m14 strain featured with reduced binding and gliding, has a substitution of amino acid conserved in glucokinase which phosphorylates glucose to glucose-6-phosphate at the first step of glycolysis (45). Interestingly, the colony of m14 is less dispersed than that of the wild-type strain, suggesting that the glucokinase is related to gliding including chemotaxis, because one of the colony shape determinants is motility in many bacteria (12). The m27 featured with the small proportion of gliding cells has a substitution at the 1461st amino acid of total 4727 in the coded Gli521 protein, suggesting that the structure around this position has an indispensable role for gliding. The m34 strain featured with the enhanced binding has a substitution in the conserved amino acid of β subunit of F-type ATPase (46). The membrane potential may be related to binding activity, because the F-type ATPase is responsible for the membrane potential in *M. mobile*.

**Cell behavior in stall.**

The cells were stalled by the optical tweezers focusing to the bead bound to the back end of cell. What events can we expect in the stall? The stall force decreased with the addition of free SL (Fig. 4). This observation suggests that the legs repeat catch, pull and release with SOs in stall rather than generate static force, because the stall force

should increase up to the stall force without SOs if the legs do not detach in stall. In our gliding model, we suggest that the leg detaches by the tension caused by the continuous cell displacement in gliding (14, 28, 41). The putative detach in the stall may suggest that the directed detach occurs in much shorter displacement than expected from the leg structure 95 nm in length. This assumption can explain the observation that *gli521* (P476R) and m34 mutants showed smaller stall force than the wild-type strain, although they have higher ratio of bound cell to glass (Fig. 2 and 3). Probably, the higher ratio of bound cell is caused by the smaller force to detach the post stroke legs.

**The unit number of gliding machinery.** The minimum force increment did not change significantly with the distance from the laser. As the force increments occurred additionally to the previous ones, the gliding unit should generate the same force constantly in a rather long distance ranging 0 to 200 nm (Fig. 6).
In the present study, we measured the stall force and the minimum force increments of a cell, which were about 113 and 1.5 pN, respectively (Fig 2*B* and 6*C*). Previously, the number of legs in *M. mobile* was estimated to be 450 (16). The number of working units was calculated from the stall force and minimum force increments of a cell, 113 over 1.5 pN is calculated to be about 75-fold, suggesting that 75 minimum units can work simultaneously. Assuming that the minimum unit of force corresponds to the single molecule of Gli349, one-sixth of Gli349 molecules are suggested to participate in the force generation in the stalled state simultaneously (Fig. 1*B*). The friction occurring at the interface between an *M. mobile* cell and water flow in the interlamellar of carp gill is calculated to be 34 pN for the maximum, based on Stokes' law (11, 47). This number is three folds smaller than the stall force of a cell, suggesting that a cell can glide against water flow using the force generated by simultaneous strokes of many legs.

***M. mobile* gliding is featured with large step and small force.** We compare the step size and the force of *M. mobile* gliding to those of conventional motor proteins such as myosin, dynein, and kinesin, which perform the stepwise movements along the rail proteins driven by the energy of ATP. The step sizes and the force of myosin-II, cytoplasmic dynein, kinesin and myosin-V have been reported as 5.3, 8, 8 and 36 nm, and 3—5, 7—8, 8 and 2—3 pN, respectively (48-53). Long step and small force of

myosin-V should be caused by the lever effect of 26-nm arms (54). The step size of *M. mobile* has been reported as 70 nm, much larger than those of the conventional motor proteins (22). The minimum unit force calculated here, 1－2 pN, suggests the gear effect in the gliding machinery. Gli521, the force transmitter forms triskelion with 100-nm arms (24) and Gli349, the leg is shaped like an eighth note in musical notation with 50-nm flexible string (26, 55), suggesting that these proteins cause the gear effect.

**Energy conversion efficiency of *M. mobile* gliding.** The direct energy source of *M. mobile* gliding has been shown as ATP, based on the experiments that permeabilized cells, "gliding ghost" can be reactivated by ATP (21). The gliding ghost showed stepwise movement with dwell time dependent on the ATP concentration used, suggesting that the step is coupled with ATP hydrolysis (22). Based on the minimum unit force of 1－2 pN and the spring constant of 0.06－0.07 pN/nm, the work done per step, $W_{step}$ was calculated as 8－33 pN nm from the equation $W_{step}$ = 1/2 × spring constant × displacement^2. Assuming that one ATP molecule is consumed per step, energy conversion efficiency of *M. mobile* gliding can be calculated around 10－40% because generally about 80 pN nm free energy is available from a hydrolysis of one ATP molecule.

F-type ATPase has been reported to reach 100% of energy conversion efficiency (56). The gliding machinery of *M. mobile* has been suggested to be driven by the α- and β-subunit paralogs of F-type ATPase (18). The force transmission from this motor to the solid surfaces through several large components including Gli521 and Gli349 may cause the loss of energy.

## Materials and methods

**Strains and Cultivation.** *M. mobile* strain 163K (ATCC 43663) as the wild type and its 9 mutants were grown in Aluotto medium at 25°C, as previously described (12, 35, 40, 57).

**Surface modifications of *M. mobile* cells and polystyrene beads.** The cultured cells were washed with PBS/G consisting of 75mM sodium phosphate (pH 7.3), 68 mM NaCl, and 20 mM glucose, suspended in 1.0 mM Sulfo-NHS-LC-LC-biotin (Thermo Scientific, Waltham, MA) in PBS/G, and kept for 15 min at room temperature (RT), as previously

306 described (28, 29, 33, 34, 40). Polystyrene beads 1.0 μm in diameter (Polysciences,
307 Warrington, PA) were coated with avidin (Sigma-Aldrich, St. Louis, MO), as previously
308 described (28).
309
310 **Force measurements.** The avidin-coated beads were attached to biotinylated cells in
311 two different ways, according to the concentrations of free SL used in experiments. In
312 force measurements under 0−0.13 mM SL conditions, the biotinylated cells were
313 inserted into a tunnel chamber which was precoated with 10% horse serum (20, 27, 29).
314 Avidin-coated beads were sonicated and inserted into the tunnel chamber with various
315 concentrations of free SL in PBS/G and bound to the cell (32). In force measurements
316 under 0.25−0.50 mM SL conditions, avidin-coated beads were sonicated and mixed with
317 biotinylated cells in a microtube, and kept for 10−30 min at RT. Then, the mixture was
318 inserted into a tunnel chamber and kept 15 min at RT. The chamber was washed with
319 PBS/G and the PBS/G was replaced by various concentrations of free SL in PBS/G.
320 Both ends of the tunnel were sealed with nail polish. The bead movements were
321 recorded at 200 or 500 frames/s and analyzed by the displacement up to 250 nm from the
322 trap center, the linear range of the laser trap, by using ImageJ 1.43u
323 (http://rsb.info.nih.gov/ij/) and IGOR Pro 6.33J (WaveMetrics, Portland, OR) (22, 28, 32,
324 58).
325
326 **Genome sequencing of various strains.** All strains were plated and isolated as
327 previously described (19). The genomic DNAs were isolated by using QIAGEN
328 DNeasy Blood & Tissue kit (QIAGEN, Hilden, Germany). The isolated genomic
329 DNA were sequenced by MiSeq (Illumina Inc., San Diego, CA) and mapped by CLC
330 Genomics Workbench 8 (QIAGEN, Hilden, Germany).
331
332 **Characterization of binding and gliding of various strains.** All strains were cultured
333 to reach an optical densities at 600 nm of 0.08. They were suspended and inserted into a
334 tunnel chamber (27, 29). The cell behaviors were recorded and analyzed as previously
335 reported (27, 35).
336
337 **ACKNOWLEDGMENTS.**
338 This work was supported by a Grant-in-Aid for Scientific Research on the Innovative
339 Area "Harmonized Supramolecular Motility Machinery and Its Diversity" (MEXT
340 KAKENHI Grant Number 24117002), and by a Grant-in-Aid for Scientific Research

(B) (MEXT KAKENHI Grant Numbers 24390107) to MM.

## References

1. Razin S, Yogev D, & Naot Y (1998) Molecular biology and pathogenicity of mycoplasmas. *Microbiol Mol Biol Rev* 62(4):1094-1156.
2. Razin S & Hayflick L (2010) Highlights of mycoplasma research--an historical perspective. *Biologicals* 38(2):183-190.
3. Miyata M (2008) Centipede and inchworm models to explain *Mycoplasma* gliding. *Trends Microbiol* 16(1):6-12.
4. Miyata M (2010) Unique centipede mechanism of *Mycoplasma* gliding. *Annu Rev Microbiol* 64:519-537.
5. Miyata M & Hamaguchi T (2016) Prospects for the gliding mechanism of *Mycoplasma mobile*. *Curr Opin Microbiol* 29:15-21.
6. Nakane D, Kenri T, Matsuo L, & Miyata M (2015) Systematic structural analyses of attachment organelle in *Mycoplasma pneumoniae*. *PLoS Pathog* 11(12):e1005299.
7. Miyata M & Hamaguchi T (2016) Integrated information and prospects for gliding mechanism of the pathogenic bacterium *Mycoplasma pneumoniae*. *Front Microbiol* 7:960.
8. Kawamoto A, *et al.* (2016) Periodicity in attachment organelle revealed by electron cryotomography suggests conformational changes in gliding mechanism of *Mycoplasma pneumoniae*. *MBio* 7(2):e00243-00216.
9. Morio H, Kasai T, & Miyata M (2015) Gliding direction of *Mycoplasma mobile*. *J Bacteriol* 198(2):283-290.
10. Lee W, *et al.* (2015) Three-dimensional superlocalization imaging of gliding *Mycoplasma mobile* by extraordinary light transmission through arrayed nanoholes. *ACS Nano* 9(11):10896-10908.
11. Miyata M, Ryu WS, & Berg HC (2002) Force and velocity of *Mycoplasma mobile* gliding. *J Bacteriol* 184:1827-1831.
12. Miyata M, *et al.* (2000) Gliding mutants of *Mycoplasma mobile*: relationships between motility and cell morphology, cell adhesion and microcolony formation. *Microbiology* 146 ( Pt 6):1311-1320.
13. Rosengarten R & Kirchhoff H (1987) Gliding motility of *Mycoplasma* sp. nov. strain 163K. *J Bacteriol* 169:1891-1898.
14. Chen J, Neu J, Miyata M, & Oster G (2009) Motor-substrate interactions in mycoplasma motility explains non-Arrhenius temperature dependence. *Biophys J*

97(11):2930-2938.

15. Uenoyama A, Kusumoto A, & Miyata M (2004) Identification of a 349-kilodalton protein (Gli349) responsible for cytadherence and glass binding during gliding of *Mycoplasma mobile*. *J Bacteriol* 186:1537-1545.
16. Uenoyama A & Miyata M (2005) Identification of a 123-kilodalton protein (Gli123) involved in machinery for gliding motility of *Mycoplasma mobile*. *J Bacteriol* 187:5578-5584.
17. Seto S, Uenoyama A, & Miyata M (2005) Identification of a 521-kilodalton protein (Gli521) involved in force generation or force transmission for *Mycoplasma mobile* gliding. *J Bacteriol* 187:3502-3510.
18. Nakane D & Miyata M (2007) Cytoskeletal "Jellyfish" structure of *Mycoplasma mobile*. *Proc. Natl. Acad. Sci. USA* 104:19518-19523.
19. Tulum I, Yabe M, Uenoyama A, & Miyata M (2014) Localization of P42 and $F_1$-ATPase alpha-subunit homolog of the gliding machinery in *Mycoplasma mobile* revealed by newly developed gene manipulation and fluorescent protein tagging. *J Bacteriol* 196(10):1815-1824.
20. Jaffe JD, Miyata M, & Berg HC (2004) Energetics of gliding motility in *Mycoplasma mobile*. *J Bacteriol* 186(13):4254-4261.
21. Uenoyama A & Miyata M (2005) Gliding ghosts of *Mycoplasma mobile*. *Proc Natl Acad Sci USA* 102(36):12754-12758.
22. Kinosita Y, *et al.* (2014) Unitary step of gliding machinery in *Mycoplasma mobile*. *Proc. Natl. Acad. Sci. USA* 111(23):8601-8606.
23. Kusumoto A, Seto S, Jaffe JD, & Miyata M (2004) Cell surface differentiation of *Mycoplasma mobile* visualized by surface protein localization. *Microbiology* 150(Pt 12):4001-4008.
24. Nonaka T, Adan-Kubo J, & Miyata M (2010) Triskelion structure of the Gli521 protein, involved in the gliding mechanism of *Mycoplasma mobile*. *J Bacteriol* 192:636-642.
25. Nagai R & Miyata M (2006) Gliding motility of *Mycoplasma mobile* can occur by repeated binding to *N*-acetylneuraminyllactose (sialyllactose) fixed on solid surfaces. *J Bacteriol* 188:6469-6475.
26. Adan-Kubo J, Uenoyama A, Arata T, & Miyata M (2006) Morphology of isolated Gli349, a leg protein responsible for *Mycoplasma mobile* gliding via glass binding, revealed by rotary shadowing electron microscopy. *J Bacteriol* 188(8):2821-2828.
27. Kasai T, *et al.* (2013) Role of binding in *Mycoplasma mobile* and *Mycoplasma pneumoniae* gliding analyzed through inhibition by synthesized sialylated

compounds. *J Bacteriol* 195:429-435.

28. Tanaka A, Nakane D, Mizutani M, Nishizaka T, & Miyata M (2016) Directed binding of gliding bacterium, *Mycoplasma mobile*, shown by detachment force and bond lifetime. *MBio* 7(3):e00455-00416.
29. Nakane D & Miyata M (2012) *Mycoplasma mobile* cells elongated by detergent and their pivoting movements in gliding. *J Bacteriol* 194:122-130.
30. Ashkin A, Dziedzic JM, Bjorkholm JE, & Chu S (1986) Observation of a single-beam gradient force optical trap for dielectric particles. *Opt Lett* 11(5):288.
31. Nishizaka T, Miyata H, Yoshikawa H, Ishiwata S, & Kinosita K, Jr. (1995) Unbinding force of a single motor molecule of muscle measured using optical tweezers. *Nature* 377:251-254.
32. Mizutani M & Miyata M (2017) Force measurement on *Mycoplasma mobile* gliding using optical tweezers. *Bio-protocol* 7(3): e2127.
33. Hiratsuka Y, Miyata M, & Uyeda TQ (2005) Living microtransporter by uni-directional gliding of *Mycoplasma* along microtracks. *Biochem Biophys Res Commun* 331(1):318-324.
34. Hiratsuka Y, Miyata M, Tada T, & Uyeda TQ (2006) A microrotary motor powered by bacteria. *Proc Natl Acad Sci U S A* 103(37):13618-13623.
35. Uenoyama A, Seto S, Nakane D, & Miyata M (2009) Regions on Gli349 and Gli521 protein molecules directly involved in movements of *Mycoplasma mobile* gliding machinery, suggested by use of inhibitory antibodies and mutants. *J Bacteriol* 191(6):1982-1985.
36. Jaffe JD, *et al.* (2004) The complete genome and proteome of *Mycoplasma mobile*. *Genome Res* 14:1447-1461.
37. Adan-Kubo J, Yoshii SH, Kono H, & Miyata M (2012) Molecular structure of isolated MvspI, a variable surface protein of the fish pathogen *Mycoplasma mobile*. *J Bacteriol* 194(12):3050-3057.
38. Wu HN, Kawaguchi C, Nakane D, & Miyata M (2012) "Mycoplasmal antigen modulation," a novel surface variation suggested for a lipoprotein specifically localized on *Mycoplasma mobile*. *Curr Microbiol* 64(5):433-440.
39. Wu HN & Miyata M (2012) Whole surface image of *Mycoplasma mobile*, suggested by protein identification and immunofluorescence microscopy. *J Bacteriol* 194(21):5848-5855.
40. Kasai T, Hamaguchi T, & Miyata M (2015) Gliding motility of *Mycoplasma mobile* on uniform oligosaccharides. *J Bacteriol* 197(18):2952-2957.
41. Kasai T & Miyata M (2013) Analyzing inhibitory effects of reagents on

*Mycoplasma* gliding and adhesion. *Bio-protocol* 3(14).

42. Leidel C, Longoria RA, Gutierrez FM, & Shubeita GT (2012) Measuring molecular motor forces in vivo: implications for tug-of-war models of bidirectional transport. *Biophys J* 103(3):492-500.
43. Ito K & Akiyama Y (2005) Cellular functions, mechanism of action, and regulation of FtsH protease. *Annu Rev Microbiol* 59:211-231.
44. Mori H & Ito K (2006) Different modes of SecY-SecA interactions revealed by site-directed in vivo photo-cross-linking. *Proc Natl Acad Sci U S A* 103(44):16159-16164.
45. Gaurivaud P, *et al.* (2016) *Mycoplasma agalactiae* secretion of beta-(1-->6)-glucan, a rare polysaccharide in prokaryotes, is governed by high-frequency phase variation. *Appl Environ Microbiol* 82(11):3370-3383.
46. Beven L, *et al.* (2012) Specific evolution of F1-like ATPases in mycoplasmas. *PLoS One* 7(6):e38793.
47. Lauder GV (1984) Pressure and water flow patterns in the respiratory tract of the bass (*Micropterus salmoides*). *Journal of Experimental Biology* 113:151-164.
48. Schnitzer MJ & Block SM (1997) Kinesin hydrolyses one ATP per 8-nm step. *Nature* 388(6640):386-390.
49. Kojima H, Muto E, Higuchi H, & Yanagida T (1997) Mechanics of single kinesin molecules measured by optical trapping nanometry. *Biophys J* 73(4):2012-2022.
50. Takagi Y, Homsher EE, Goldman YE, & Shuman H (2006) Force generation in single conventional actomyosin complexes under high dynamic load. *Biophys J* 90(4):1295-1307.
51. Fujita K, Iwaki M, Iwane AH, Marcucci L, & Yanagida T (2012) Switching of myosin-V motion between the lever-arm swing and brownian search-and-catch. *Nat Commun* 3:956.
52. Park PJ & Lee KJ (2013) A modified active Brownian dynamics model using asymmetric energy conversion and its application to the molecular motor system. *J Biol Phys* 39(3):439-452.
53. Gennerich A, Carter AP, Reck-Peterson SL, & Vale RD (2007) Force-induced bidirectional stepping of cytoplasmic dynein. *Cell* 131(5):952-965.
54. Vilfan A (2005) Elastic lever-arm model for myosin V. *Biophys J* 88(6):3792-3805.
55. Metsugi S, *et al.* (2005) Sequence analysis of the gliding protein Gli349 in *Mycoplasma mobile*. *Biophysics (Nagoya-shi)* 1:33-43.
56. Kinosita K, Jr., Yasuda R, Noji H, & Adachi K (2000) A rotary molecular motor that can work at near 100% efficiency. *Philos Trans R Soc Lond B Biol Sci*

355(1396):473-489.

57. Aluotto BB, Wittler RG, Williams CO, & Faber JE (1970) Standardized bacteriologic techniques for the characterization of *Mycoplasma* species. *Int. J. Syst. Bacteriol.* 20:35-58.
58. Kinosita Y, Uchida N, Nakane D, & Nishizaka T (2016) Direct observation of rotation and steps of the archaellum in the swimming halophilic archaeon *Halobacterium salinarum*. *Nat Microbiol* 1(11):16148.

## Figure legends

**Fig. 1.** Schematic illustration of gliding machinery. (*A*) Magnified illustration of unit. The single unit consists of internal structure (upper blue) and three huge proteins, Gli123 (purple), Gli349 (red) and Gli521 (green) on the cell surface. The force generated by the internal structure based on ATP hydrolysis transmits through Gli521 and pulls Gli349 repeatedly. Gli349 catches and pulls SOs on the solid surface, and the unit force was estimated around 1.5 piconewton (pN) in the present study (see Fig. 6). (*B*) About 75 legs (red) sticking out from the cell work simultaneously. The cell glides in the direction of yellow arrow. Only bound legs are illustrated.

**Fig. 2.** Stall force of various strains. (*A*) Left: Illustration and micrograph of measurement by using optical tweezers. The polystyrene bead (circle) 1 μm in diameter bound to the cell was trapped by a focused laser beam (yellow hourglass) and glides to the direction of white arrow. Black and pink crosses indicate a focal point of laser and a bead center, respectively. Right: Optical micrographs of trapped cell. The cell with bead (large black ring with white center) was trapped at 0 s and stalled at 80 s. (*B*) Representative traces. The line colors correspond to the bars in the inset. Inset: Averages were normalized by the WT value, and presented with standard deviations (SD) ($n$ = 50, 42, 26, 31 and 35). **, $P < 0.01$ (The difference from WT was supported by Student's $t$-test).

**Fig. 3.** Binding and gliding properties of various strains. (*A*) The cell trajectories were presented as a stack for 5 s, changing its color from red to blue. (*B*) Averages of

binding activity (right) and gliding speed (left) were normalized by the WT value and presented with SD.

**Fig. 4.** Efficiency of SO on stall force. (*A*) Representative traces in various concentrations of SL. (*B*) Concentration dependency on SL. Averages were plotted with SD ($n$ = 50, 13, 23, 16, 16 and 11 for 0, 0.05, 0.13, 0.25, 0.33 and 0.50 mM, respectively).

**Fig. 5.** Detection of force increments under low load and 0.25 mM SL. (*A*) Representative traces of force transition in WT and *gli521* (P476R) mutant shown in upper and lower panels, respectively. Green and cyan triangles in each panel indicate small peak positions taken by a peak-finding algorithm. (*B*) Distributions of peak values detected by the peak-finding algorithm were fitted by the sum of four Gaussian curves. The first, second, third and fourth tops of Gaussian curves are 1.1, 2.0, 3.2 and 4.4 pN in WT, and 1.0, 1.8, 2.6 and 3.5 pN in *gli521* (P476R) mutant, respectively ($n$ = 976 and 1067).

**Fig. 6.** Detection of force increments under low load and 0.50 mM SL. (*A*) Two representative time courses of force generation. The trajectories in dashed rectangular areas are magnified as insets and marked green and blue lines for increments and dwell times. (*B*) Representative time course of continuous stepwise trajectory. The histogram of PDF analysis for indicated steps was shown in right inset. (*C*) The histogram of force increments for 46 steps or peaks. The averaged value was indicated by a black triangle.

**Fig. S1.** Distributions of gliding speed of various strains in 10 s. Experimental data were fitted by the sum of two Gaussian curves colored in blue.

**Movie S1.** Stall force of gliding cell carrying a bead measured by optical tweezers.

**Movie S2.** Stepwise movement of gliding cell carrying a bead detected with weak trap.

# Fig. 1.

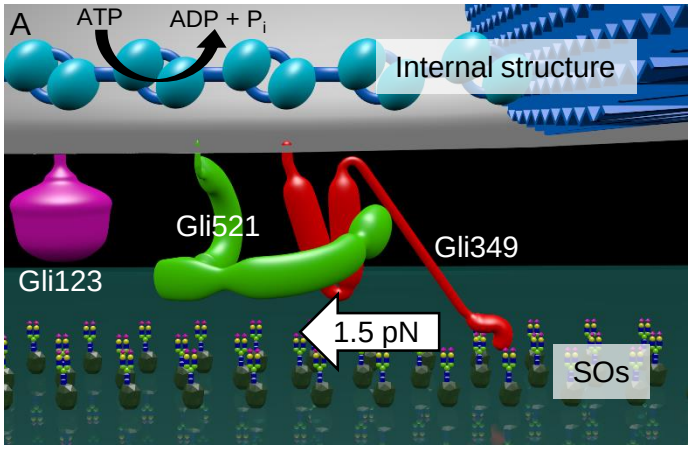


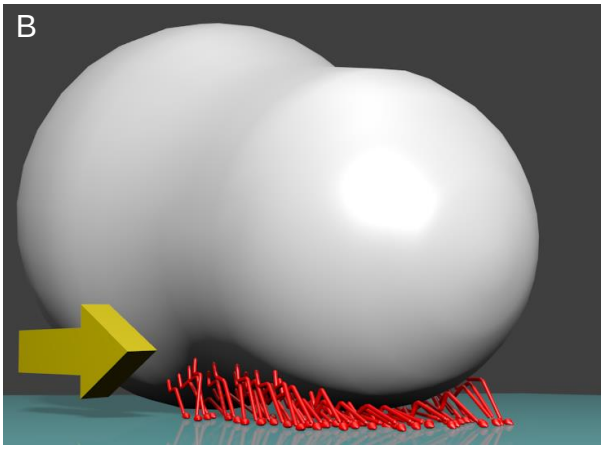

# Fig. 2.

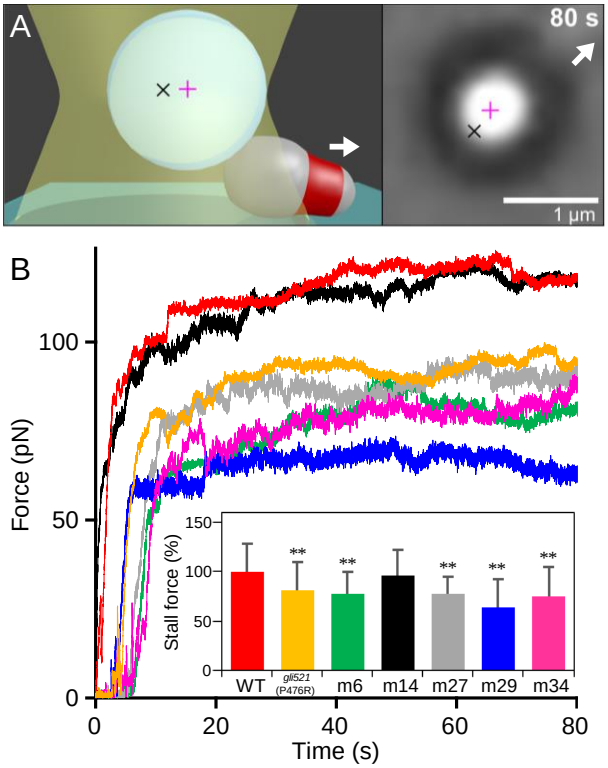

# Fig. 3.

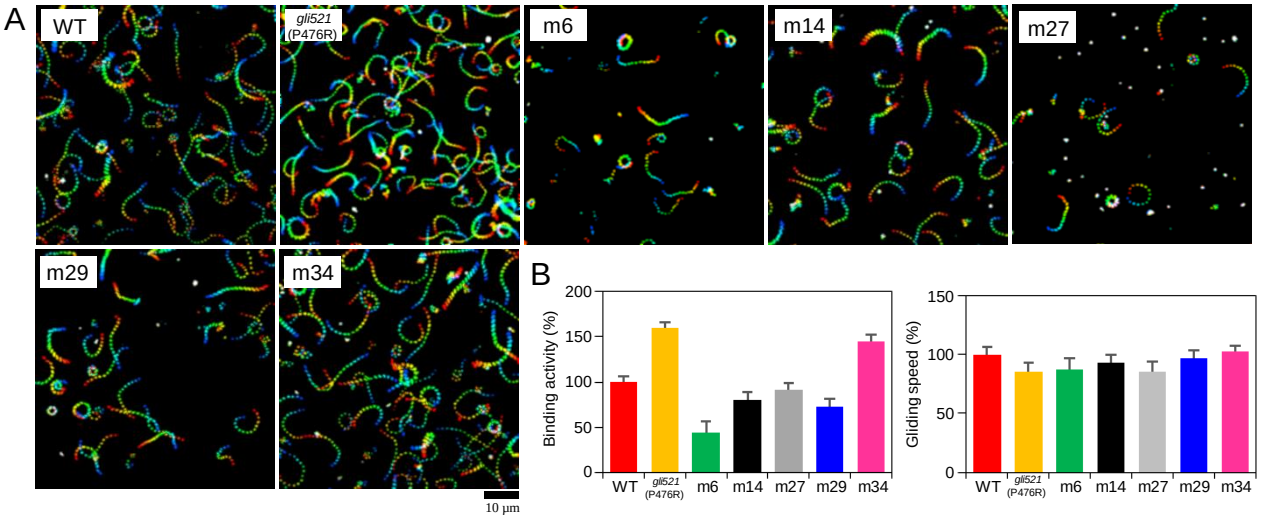

# Fig. 4.

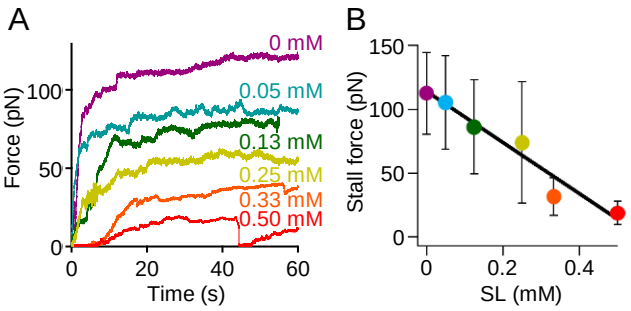

# Fig. 5.

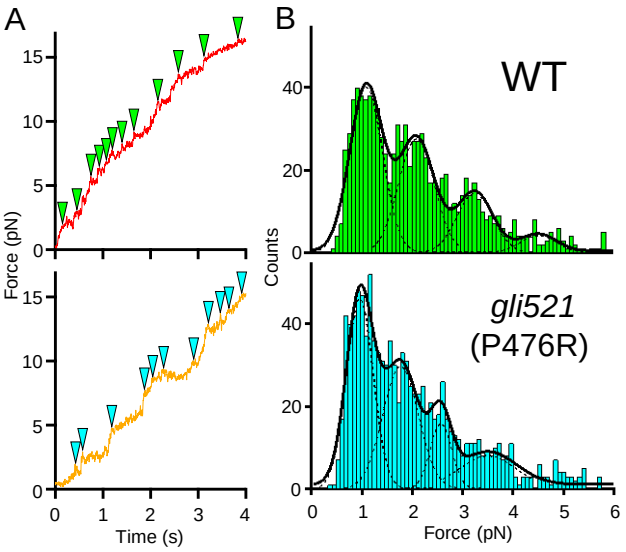

# Fig. 6.

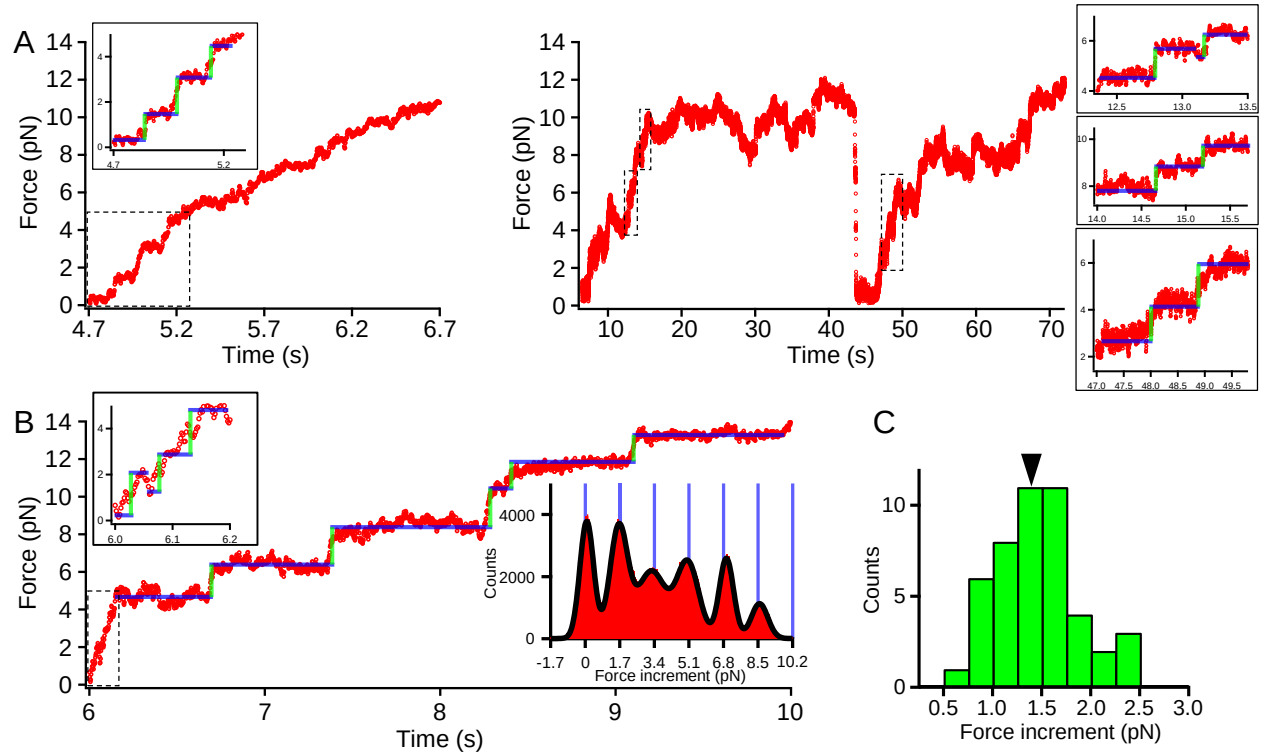

# Fig. S1.

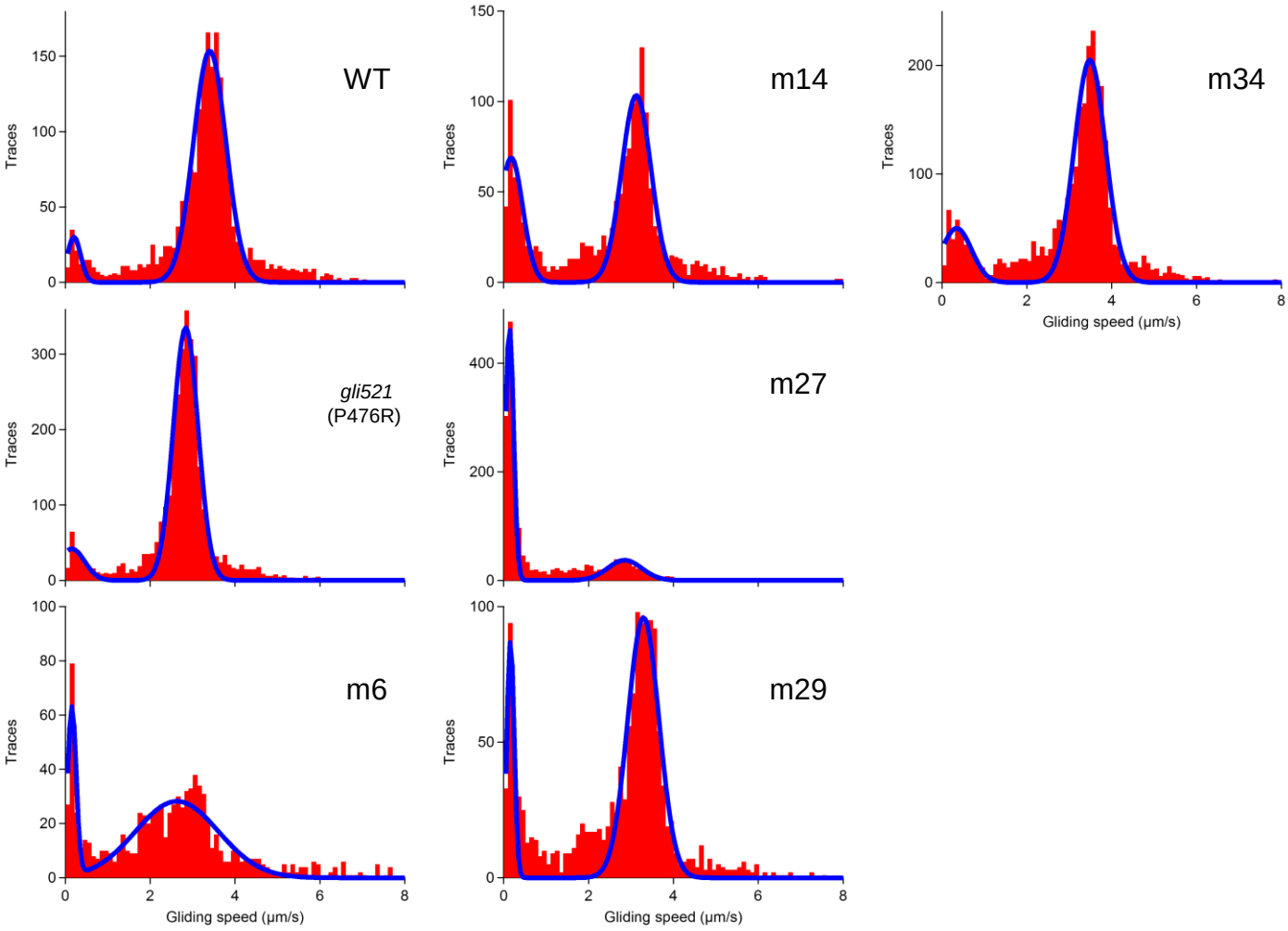

**TABLE 1** Whole genome sequence of various strains

| Strain | Nucleotide change[a] | Amino acid change[b] | Previously reported | Mutation type | ORF | Annotation[c] |
|---|---|---|---|---|---|---|
| WT | C232735A | S354I | | missense | MMOB1700 | Hypothetical |
| *gli521* (P476R) | C149908G | P476R | P476R | missense | MMOB1040 | Gli521 |
| | C232735A | S354I | | missense | MMOB1700 | Hypothetical |
| | 399903T399904 | M8−36* | | frame shift | MMOB3220 | MvspB |
| m6 | C232735A | S354I | | missense | MMOB1700 | Hypothetical |
| | G308962A | G350R | | missense | MMOB2540 | SecY preprotein translocase subunit |
| | C423006- | E225−230* | | frame shift | MMOB3340 | MvspI |
| | G676032C | P191R | | missense | MMOB5400 | FtsH |
| m12 | C136968T | Q523* | Q523* | nonsense | MMOB1020 | Gli123 |
| | T214208- | F672−695* | | frame shift | MMOB1570 | Oligopeptide ABC transporter binding protein |
| | C232735A | S354I | | missense | MMOB1700 | Hypothetical |
| | A232903T | I298N | | missense | MMOB1700 | Hypothetical |
| | C424498A | H195N | | missense | MMOB3350 | PolC truncated DNA polymerase III |
| m13 | C142646T | Q1257* | Q1257* | nonsense | MMOB1030 | Gli349 |
| | C232735A | S354I | | missense | MMOB1700 | Hypothetical |
| m14 | C232735A | S354I | | missense | MMOB1700 | Hypothetical |
| | 233458T233459 | I113−142* | | frame shift | MMOB1700 | Hypothetical |
| | C272657A | P156Q | | missense | MMOB2030 | Glucokinase |
| m23 | C147186T | S2770L | S2770L | missense | MMOB1030 | Gli349 |
| | T214208- | F672−695* | | frame shift | MMOB1570 | Oligopeptide ABC transporter binding protein |
| | C232735A | S354I | | missense | MMOB1700 | Hypothetical |
| | A233098C | I233S | | missense | MMOB1700 | Hypothetical |
| | A345995T | N18Y | | missense | MMOB2830 | HsdR Type I restriction enzyme r protein |
| m27 | A73556G | L101L | | silent | MMOB0550 | Frr ribosome recycling factor |
| | C152863T | P1461L | | missense | MMOB1040 | Gli521 |
| | C232735A | S354I | | missense | MMOB1700 | Hypothetical |
| m29 | C232735A | S354I | | missense | MMOB1700 | Hypothetical |
| | A587414T | K29N | | missense | MMOB4660 | TruB tRNA pseudouridine synthase B |
| | C654504T | W82* | | nonsense | MMOB5190 | Hypothetical |
| | A754250- | I126* | | frame shift | MMOB6120 | Hypothetical |
| m34 | C232735A | S354I | | missense | MMOB1700 | Hypothetical |
| | A232753G | I348T | | missense | MMOB1700 | Hypothetical |
| | T365326A | D304V | | missense | MMOB2960 | AtpD $F_oF_1$ ATPase beta subunit |

[a] Numbering is as in the sequence under accession number NC_006908.
[b] Asterisks indicate stop codons.
[c] Annotations are based on Molligen 3.0.